Electronic Supplementary Information

Controlling defects in crystalline carbon nitride to optimize photocatalytic CO_2 reduction

Han Li, Bicheng Zhu, Shaowen Cao,* and Jiaguo Yu*

State Key Laboratory of Advanced Technology for Materials Synthesis and Processing, Wuhan University of Technology, 430070 Wuhan, P. R. China

E-mail: swcao@whut.edu.cn; jiaguoyu@yahoo.com

Experimental section

Preparation of pristine CN and crystalline CN

Pristine CN was prepared by using melamine as the starting material. Melamine (1 g) was heated at 600 °C in air for 4 h with a ramp rate of 3 °C min^{-1}. After that, a light yellow powder was obtained and denoted as CN. Crystalline CN was prepared by molten-salt method. Melamine powder (1 g) and NaCl were uniformly mixed in a mortar with a mass ratio (1:10), then placed in a covered quartz boat. Then the quartz boat was placed in a tube furnace, calcined in nitrogen gas atmosphere to 600°C with a heating rate of 3 °C min^{-1}, kept at 600 °C for 4 h. The resulting yellow powder was dissolved in 1 L deionized water, stirred for 12 h, washed thoroughly, and dried under vacuum at 60 °C for 12 h. The obtained product was denoted as CN-M.

Preparation of defect modified crystalline CN (CN-M-x)

1 g of melamine powder was added into aqueous KOH solutions (0.005-0.02 g KOH in 20 mL H_2O), evaporated to dryness with an oil bath at 85 °C. The solid mixture of melamine, KOH and NaCl were uniformly mixed in a mortar with a mass ratio (1: x: 10, where x=0.005, 0.01, 0.02). Then the solid mixture was placed in a covered quartz boat, and calcined in nitrogen gas atmosphere to 600°C with a heating rate of 3°C min^{-1}, kept at 600 °C for 4 h. The resulting yellow powder was dissolved in 1 L deionized

water, stirred for 12 h, washed thoroughly, and dried under vacuum at 60 °C for 12 h. The as-prepared products were denoted as CN-M-x (where x =0.005, 0.01, 0.02).

Characterization

The XRD patterns were measured by D/Max-RB X-ray diffractometer using a Cu Kα radiation with a range of 5-80°. UV-vis DRS of the samples were obtained on a UV-vis spectrometer (UV-2600, Shimadzu). Morphological observations of the samples were conducted by a field emission scanning electron microscope (FESEM, JSM 7500F) and a double-corrected JEOL ARM200F transmission electron microscope (TEM). The thickness of CN-M-0.01 nanosheet was determined on a multimode 8 atomic force microscopic (AFM, Bruker, USA) equipment in tapping mode. The Fourier transfer infrared (FTIR) spectra of the samples were recorded by an IR Affinity-1 FTIR spectrometer. Photoluminescence (PL) emission spectra were observed on a Fluorescence Spectrophotometer (F-7000, Hitachi, Japan) with an excitation wavelength of 360 nm. The Na and K contents were measured using atomic absorption spectrometer (contrAA-700, Jena, Germany). Nitrogen adsorption–desorption isotherms were measured using a Micromeritics ASAP 2020 nitrogen adsorption apparatus. All the samples were degassed before adsorption measurements. The Brunauer–Emmett–Teller (BET) specific surface area (S_{BET}) of all the samples was obtained by the multipoint Brunauer–Emmett–Teller (BET) method. CO_2 temperature programmed desorption (TPD) measurements were conducted on the BELCAT-B (Japan) instrument. In a typical experiment, 50 mg of sample was first pretreated with helium gas (50 mL min−1) at 200 °C for 30 min and cooled down to 50 °C, and flowed with CO_2 gas for 30 min. After that, it was purged with helium gas for 1 h at 50 °C to remove weakly adsorbed CO_2. Then the temperature was ramped to 500 °C at 10 °C min−1 under the flow of helium gas (30 mL min^{-1}). The chemical compositions and states of the samples were confirmed by X-ray photoelectron spectroscopy (XPS), which was equipped with an ultrahigh vacuum VG EXCALAB 210 electron spectrometer by using Al Kα radiation as the X-ray source. All binding energies were referenced to the C 1s peak of adventitious carbon at 284.8 eV. The

photoelectrochemical measurements were performed on a CHI660C workstation using a standard three-compartment electrochemical cell with a platinum coil and an Ag/AgCl as counter and reference electrodes correspondingly. The samples coated on an FTO glass served as the working electrode. All the electrodes were placed in 0.5 M Na_2SO_4 aqueous solution. The EIS was performed at −0.06 V versus Ag/AgCl. Time-resolved photoluminescence (TRPL) spectra were measured on a FLS920 fluorescence lifetime spectrophotometer (Edinburgh Instruments, UK) with an excited wavelength at 360 nm. Carbon monoxide and Methane labeled by ^{13}C and ^{12}C were detected with a gas chromatography-mass spectrometer (Agilent Technologies 7890B GC system with 5977B MSD, USA). the electron paramagnetic resonance (EPR) spectra were performed on an EPR spectrometer (MEX-nano, Bruker) with a modulation frequency of 100 kHz and a microwave power of 25 mW. The NMR experiment was carried out on a Bruker-500 (Bruker, Germany) using the $^1H \rightarrow {}^{13}C$ solid-state cross-polarization/magic angle spinning nuclear magnetic resonance (CP/MAS NMR) technique with the MAS spinning speed of 8 kHz, equipped with a double resonance 4 mm probe. The chemical shifts were referenced to hexamethylbenzene (HMB) for ^{13}C.

Photocatalytic CO_2 reduction measurements

The reaction was carried out using a bottle of a two-neck Pyrex reactor with two parallel planes. 0.05 g of sample was put onto the bottom of the Pyrex reactor with deionized water, then dried at 80 °C. The wet CO_2 was blown through the reactor for 30 min to ensure anaerobic conditions of the reaction system and used as CO_2 and H_2O sources. Thereafter, the Pyrex reactor was irradiated under a 300 W Xe lamp with an AM1.5 filter (100 mw/cm^2). Then the gas products were detected and measured by the gas chromatograph (GC-14C, SHIMADZU, JAPAN). Particularly, the GC used for the detection of CH_3OH is equipped with a capillary column (Agilent DB-WAX, 30 m, 0.18 mm). And the temperature of the injection port, column, and detector is 70, 120 and 160 °C, respectively. Another GC used for the detection of CO and CH_4 is equipped with a packed column (Sailuxin Instrument, 2m, 2mm), and the temperature of the injection port, column, and detector is 70, 120 and 250 °C, respectively.

The equations of fitting luminescence decay curves and calculating the average lifetime

The equation which is used to fit luminescence decay curves:

$$I(t)=I_0+\sum_{i=1}^{n=3} A_i \exp\left(\frac{-t}{\tau_i}\right)$$

where $I(t)$ is the PL intensity at a given time, I_0 is a baseline correction, and A_i and τ_i are the preexponential factors and excited-state luminescence decay time associated with the ith component, respectively.

The equation which is used to calculate the average lifetime τ_{av}:

$$\tau_{av} = \frac{A_1\tau_1^2 + A_2\tau_2^2 + A_3\tau_3^2}{A_1\tau_1 + A_2\tau_2 + A_3\tau_3}$$

Calculation of selectivity

The selectivity of photocatalytic CO_2 reduction to valuable fuels was calculated using the following equation:

$$\text{Selectivity of valuable hydrocarbons (\%)}=\frac{2n(CO)+6n(CH_3OH)+8n(CH_4)}{2n(CO)+6n(CH_3OH)+8n(CH_4)+2n(H_2)}\times100\%$$

Where $n(CO)$, $n(CH_4)$, $n(CH_3OH)$ and $n(H_2)$ are the amounts (moles) of CO, CH_4, CH_3OH and H_2 formed within a certain period of time.

Quantum yield calculation

The photochemical quantum yield (Φ) is an important parameter to characterize the photoreduction performance. The light intensity in the effective range (280 to 450 nm) was estimated from the measured light spectrum of the 300 W Xe lamp with an AM1.5 filter in this work (Fig. S12) using the following equation:

$$P = \int_{\lambda_m}^{\lambda_n} f(\lambda)d\lambda = \sum_{i=m}^{i=n}(\frac{A_m+A_n}{2})\bullet\Delta\lambda$$

Where λ is the wavelength (nm), A_m and A_n provide the simulated solar spectral irradiance ($\mu W\ m^{-2}\ nm^{-1}$) in the wavelength of λ_m and λ_n. Thus, the average wavelength in the effective range (280 to 450 nm) was estimated to be 329 nm.

The photon energy at a certain wavelength is calculated using the following equation:

$$E_{photon} = \frac{hc}{\lambda}$$

Where h is the Plank constant, c is the speed of light, and λ is the wavelength. The average photon energy is estimated by using the average wavelength in the range of 280 to 450 nm. The deposited catalyst film area (S) is $23.7 cm^2$.

The mole of photo absorbed by catalyst (n) is calculated using the following equation:

$$n = \frac{P \times S \times t}{N_A \times E_{photon}}$$

Where P is the light intensity, S is the catalyst film area, t is the irradiation time, NA is the Avogadro's constant. Therefore, quantum yields of CO, CH4, and CH3OH can be calculated using the following equations.[1,2] Two, eight, six electrons are required to convert CO_2 to CO, CH4, and CH3OH, respectively.

$$\Phi_{co}(\%) = \frac{2\ mol\ of\ CO\ yield}{moles\ of\ photon\ absorbed\ by\ catalyst} \times 100\% \quad (1)$$

$$\Phi_{CH_4}(\%) = \frac{8\ mol\ of\ CH_4\ yield}{moles\ of\ photon\ absorbed\ by\ catalyst} \times 100\% \quad (2)$$

$$\Phi_{CH_3OH}(\%) = \frac{6\ mol\ of\ CH_3OH\ yield}{moles\ of\ photon\ absorbed\ by\ catalyst} \times 100\% \quad (3)$$

Computational details

The density functional theory (DFT) calculations were carried out by using the Vienna Ab initio Simulation Package (VASP). The exchange–correlation interaction was described by generalized gradient approximation (GGA) with the Perdew–Burke–Ernzerhof (PBE) functional. The energy cutoff and Monkhorst–Pack k-point mesh were set as 500 eV and $3 \times 3 \times 1$, respectively. The convergence criteria were set as 10^{-5} eV for energy and 0.01 eV/Å for force. For the construction of surface models, a vacuum of 20 Å was used to eliminate interactions between periodic structures. The van der Waals interaction was described using DFT-D2 method of Grimme. Pristine CN-M is a

2×2 supercell consisting of 24 C and 32 N atoms. To simulate N vacancy and cyano contained CN-M, a two-coordinated N atom and a tri-s-triazine unit in the 2×2 supercell were deleted. Three bridging N atoms were therefore exposed. Two of them were saturated by H atoms, the other one was grafted by a C≡N group.

Table S1. The contents of Na and K over CN-M and CN-M-0.01 measured by atomic absorption spectroscopy.

Sample	Na (wt%)	K (wt%)
CN-M	1.60	\
CN-M-0.01	1.67	0.18

Table S2. XPS peak areas of CN and CN-M-0.01

Sample	C–N=C (peak area)	N–(C)$_3$ (peak area)
CN-M	4842	1254
CN-M-0.01	6470	2293

Table S3. Physical properties of CN, CN-M, CN-M-0.005, CN-M-0.01 and CN-M-0.02.

Sample	S_{BET} (m^2 g^{-1})	Pore volume (cm^{3}g^{-1})	Average pore size (nm)
CN	23	0.11	17.9
CN-M	12	0.04	14.0
CN-M-0.005	30	0.13	20.0
CN-M-0.01	31	0.12	12.7
CN-M-0.02	34	0.12	13.8

Table S4. The radiative fluorescence lifetimes and relative percentages.

Sample	τ_{av}	τ_1(ns) (rel. %)	τ_2(ns) (rel. %)	τ_3(ns) (rel. %)
CN	15.36	1.56(25)	4.64(45)	19.99(30)
CN-M	9.13	1.25(18)	3.70(54)	12.68(28)
CN-M-0.01	11.10	1.42(22)	4.10(55)	16.16(23)

Table S5. The yield of gas products ($\mu mol\ g^{-1}\ h^{-1}$) of CN, CN-M, CN-M-0.005, CN-M-0.01 and CN-M-0.02, without any sacrificial agent.

Sample	CO	CH_4	CH_3OH	Total CO_2 conversion[a]	H_2	CO_2 photoreduction selectivity (%)
CN	1.83	1.25	0.13	3.21	2	78.3%
CN-M	3.53	3.52	0.59	7.64	trace	~100%
CN-M-0.005	6.57	1.76	0.24	8.57	trace	~100%
CN-M-0.01	10.6	2.75	0.19	13.54	trace	~100%
CN-M-0.02	5.42	1.43	0.27	7.12	trace	~100%

[a]Total CO_2 conversion = $n(CH_4) + n(CO) + n(CH_3OH)$

Table S6. Comparison of the photocatalytic CO_2 reduction activities of polymeric carbon nitride based photocatalysts.

Photocatalyst	Light source	Dosage	CO (μmol g^{-1} h^{-1})	CH$_4$ (μmol g^{-1} h^{-1})	CH$_3$OH (μmol g^{-1} h^{-1})	Year	Ref
Defective crystalline carbon nitride	350W Xe lamp (AM1.5 filter)	100 mg	1.12	6.24	3.85	2019	3
Hierarchical 3D porous g-C$_3$N$_4$	300W Xe lamp	100 mg	11.2	0.45	\	2019	4
Hierarchical flower-like g-C$_3$N$_4$	300W Xe lamp	30 mg	18.8	1.8	\	2019	5
Phosphorus-doped g-C$_3$N$_4$ nanotube	300W Xe lamp	50 mg	2.37	1.81	\	2018	6
B-doped g-C$_3$N$_4$	300W Xe lamp	50 mg	0.45	0.16	\	2019	7
Carbon nitride with tailoring grain boundary	350W Xe lamp (AM1.5 filter)	50 mg	14.2	1.2	0.5	2019	8
g-C$_3$N$_4$ scaffold with C(CN)$_3$ cocatalyst	300W Xe lamp	100 mg	16.5	0.2	\	2020	9
NiAl-LDH/g-C$_3$N$_4$	300W Xe lamp (λ>420 nm)	50 mg	8.2	\	\	2018	10
Defect modified crystalline carbon nitride	300W Xe lamp (AM1.5 filter)	50 mg	10.6	2.75	0.19	2020	This work
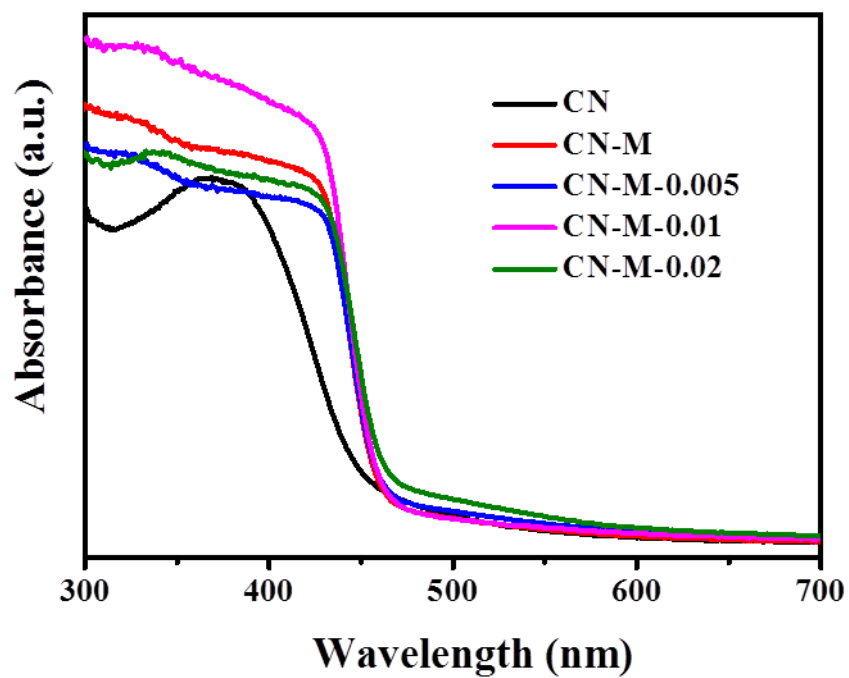
Fig. S1 UV-vis diffuse reflectance spectra (DRS) of CN, CN-M, CN-M-0.005, CN-M-0.01 and CN-M-0.02.
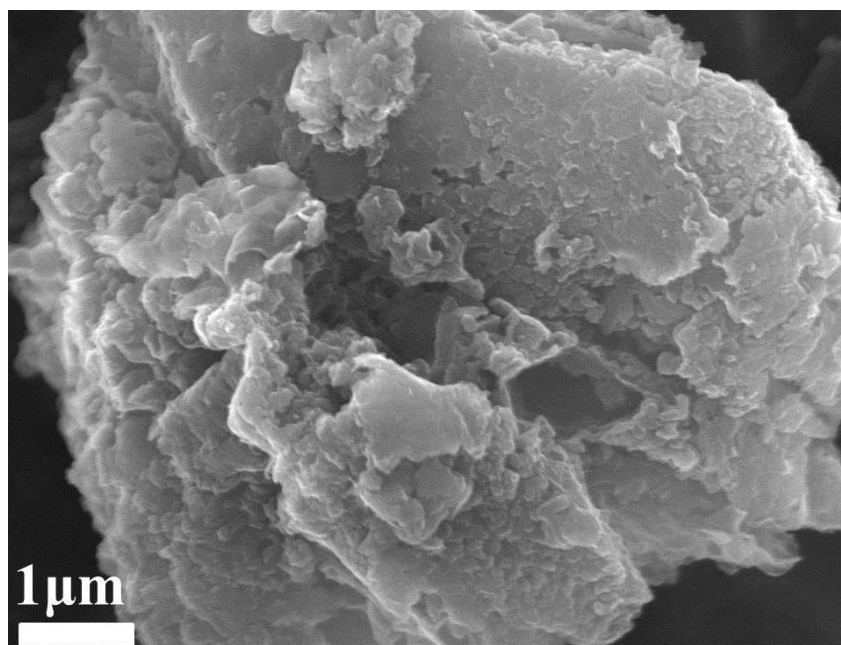

**Fig. S2** Field emission scanning electron microscopic (FESEM) image of CN.
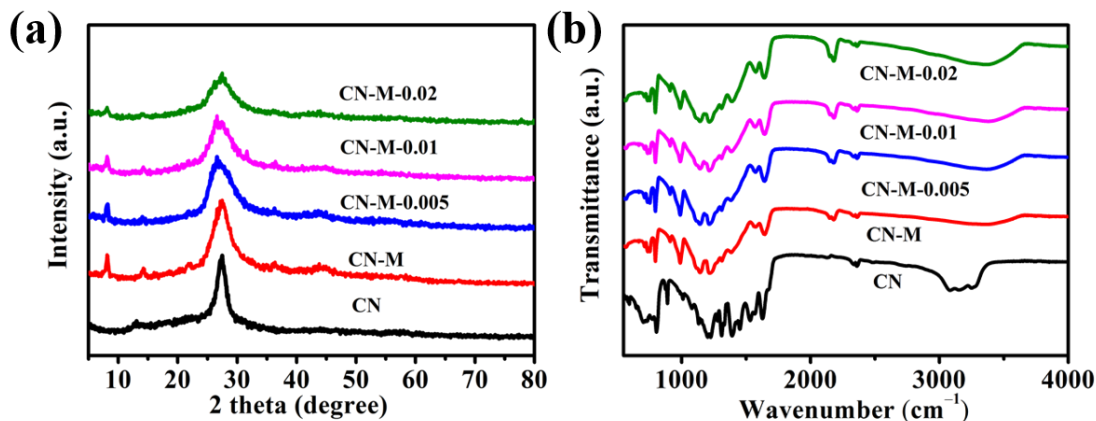
Fig. S3 (a) X-ray diffraction (XRD) patterns and (b) FTIR spectra of CN, CN-M, CN-M-0.005, CN-M-0.01, and CN-M-0.02.

XRD pattern of CN (see Fig. S3a) shows two typical diffraction peaks at 27.3° and 13.3°, corresponding to (002) and (100) planes, respectively. The main diffraction peak (002) is a characteristic interlayer stacking peak of graphitic-like structure. The low-angle diffraction peak (100) originates from the repeated structural packing of tri-s-triazine heterocycles.[11]

FTIR spectrum (see Fig. S3b) of CN shows a sharp peak at 810 cm^{-1}, which is characteristic of the breathing mode of N-containing heterocycles. While the peaks from 900 cm^{-1} to 1800 cm^{-1} belong to the stretching modes of C–N band in the N-containing heterocycles.[12] The peaks between 2900 cm^{-1} to 3500 cm^{-1} are ascribed to N–H stretching or O–H stretching.

11
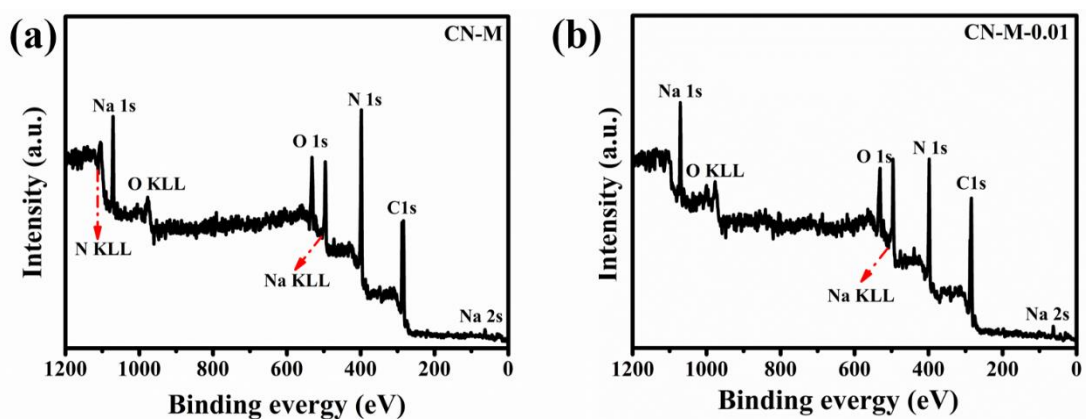
**Fig. S4** (a) XPS survey spectra of CN-M (b) XPS survey spectra of CN-M-0.01.
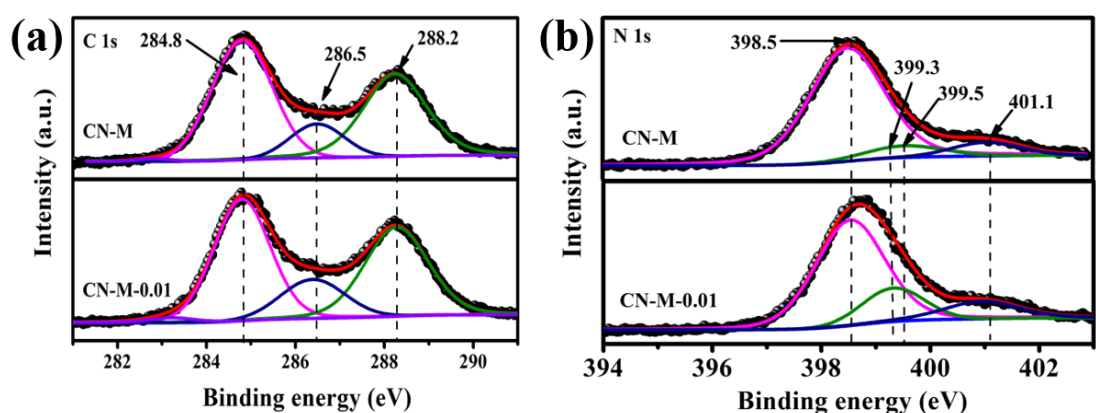
Fig. S5 High-resolution XPS spectra of C 1s (a) and N 1s (b) of CN-M, CN-M-0.01.

The high resolution of C 1s in the CN-M with a binding energy of 288.2 eV, 286.5 eV and 284.8 eV are assigned to the sp^2 C atom bonded to N inside the s-triazine rings, sp^2 C atom in the aromatic ring attached to the $-NH_2$ groups and the impurities of graphitic carbon species, respectively (Fig. S5a).[11,13] The C 1s peak intensity of CN-M-0.01 at 286.5 eV is enhanced, which is an additional evidence for the formation of C≡N groups, as the cyano groups possess the similar binding energy with $C-NH_2$. In Fig. S5b, the N 1s spectrum of CN-M can be deconvoluted into three peaks at 398.5, 399.5 and 401.1, which are assigned to sp^2-hybridized nitrogen bonded to C (C–N=C), sp^3 tertiary nitrogen (N–(C)$_3$) and the hydrogen-bearing amine (C–N–H), respectively.[14]
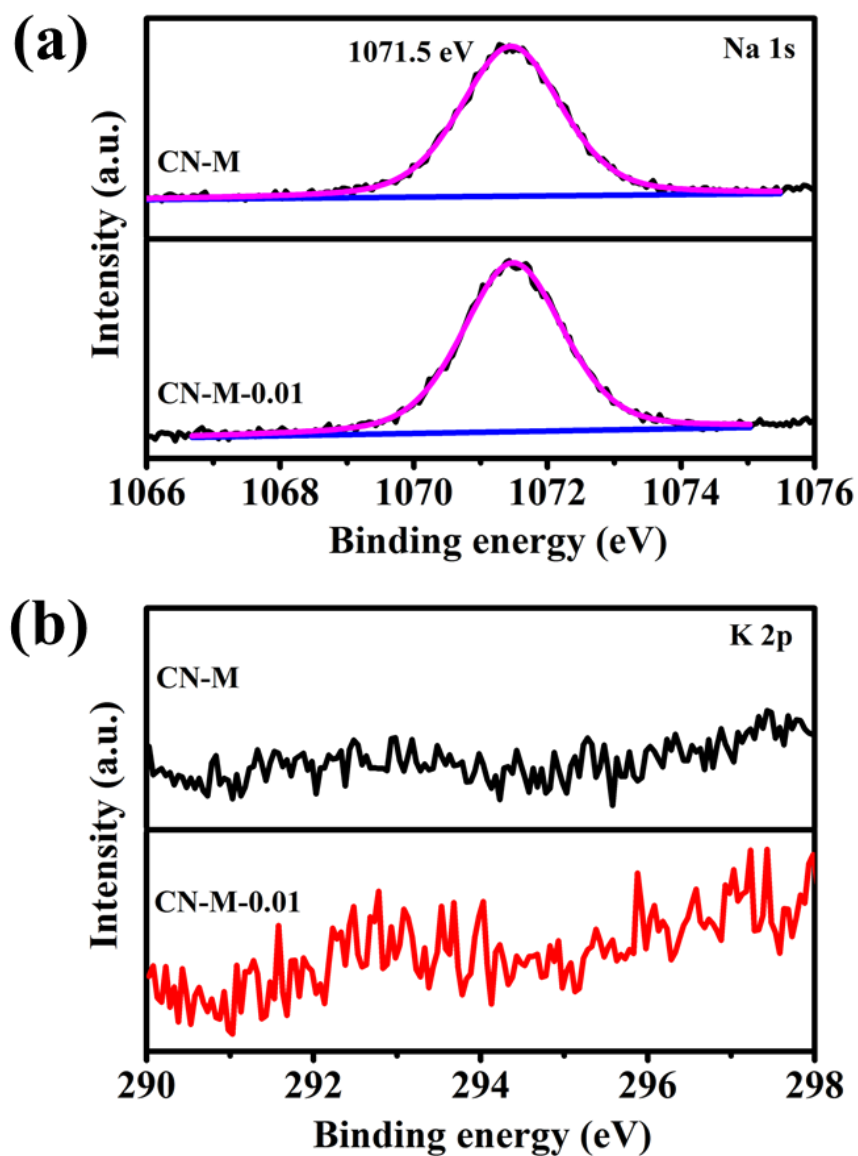
Fig. S6 High-resolution XPS spectra of a) Na 1s and b) K 2p.

No signal corresponding to K 2p was found for the samples. The positive Na+ could be balanced mainly by the N atom via Na–N bonds, which is in agreement with the FTIR results.[15]
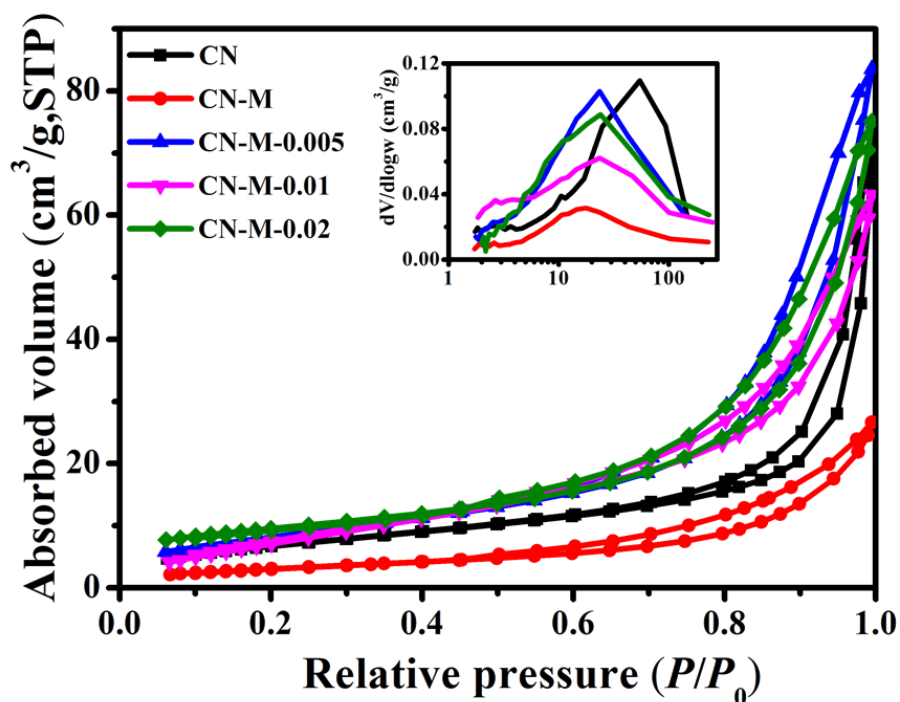
Fig. S7 N_2 adsorption–desorption isotherms of CN, CN-M, CN-M-0.005, CN-M-0.01, CN-M-0.02 and the inset displaying the corresponding pore-size distribution curves.

The N_2 sorption measurements show that all the samples including CN and CN-M-x are featured by a typical IV isotherm with a H3 type hysteresis loop, suggesting the formation of slit-like pores, originated from the stacking and aggregation of nanosheets.[16] All the pore size distribution curves show a wide distribution in the range of 2-100 nm.
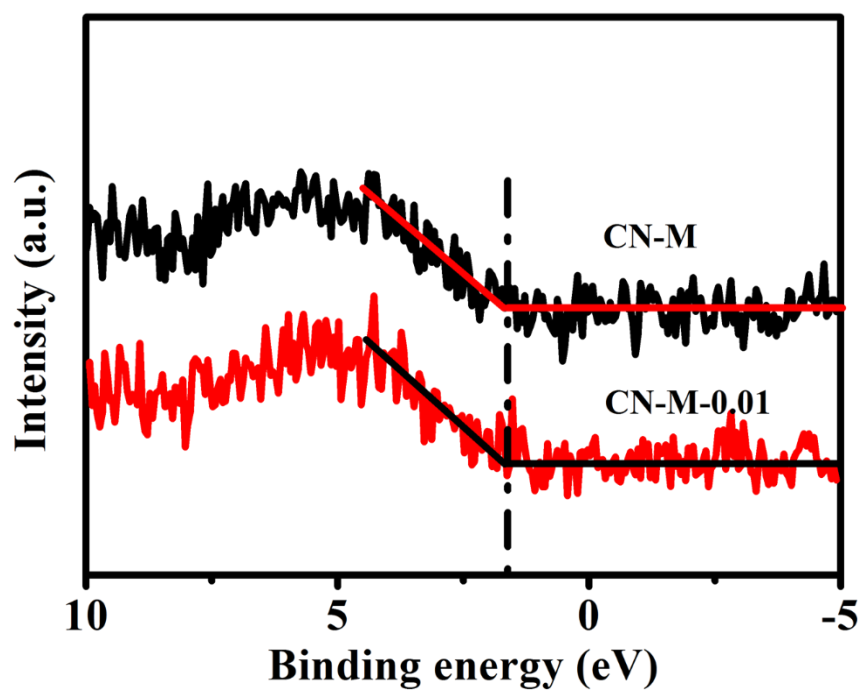
Fig. S8 XPS valence band (VB) spectra of CN-M and CN-M-0.01. The VB potentials of CN-M and CN-M-0.01 calculated by the XPS valence band spectra are both located at 1.61 eV.
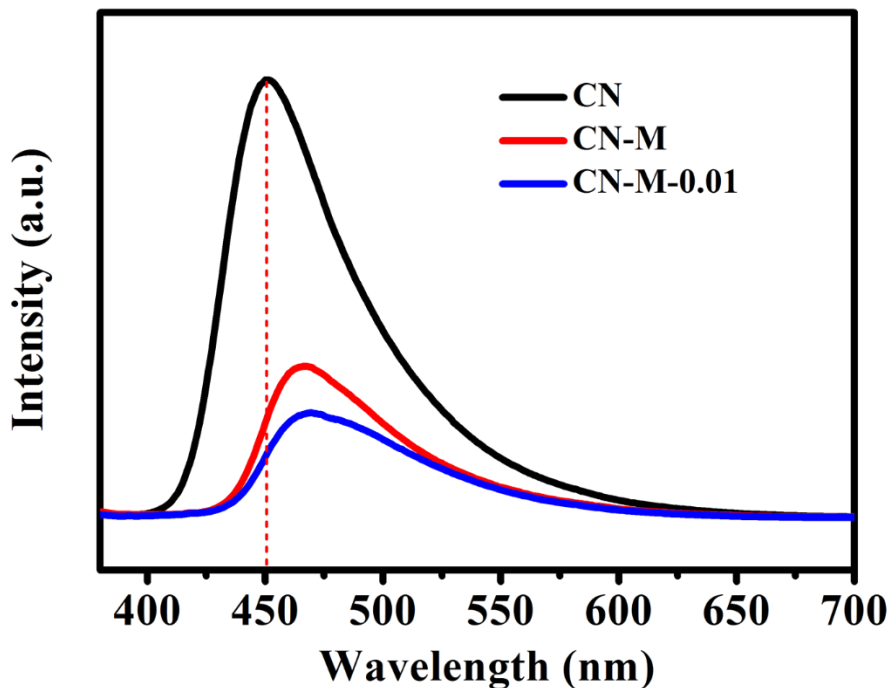
**Fig. S9** PL spectra of CN, CN-M, CN-M-0.005, CN-M-0.01 and CN-M-0.02 excited at the wavelength of 360 nm.

The steady-state PL peak of CN is at 450 nm, corresponding to the absorption edge in the UV-vis DRS and indicating the luminescence of pristine carbon nitride mainly originates from band edge recombination. The PL peak of CN-M is located at 460 nm, which is red-shift with reference to that of CN, consistent with the red shift of absorption edge in the UV-vis DRS. The peak intensity is greatly decreased, implying the high crystallinity already favours the efficient electron transfer. The PL peak intensity of CN-M-0.01 further decreases, indicating the defects promote the separation of electrons and holes.
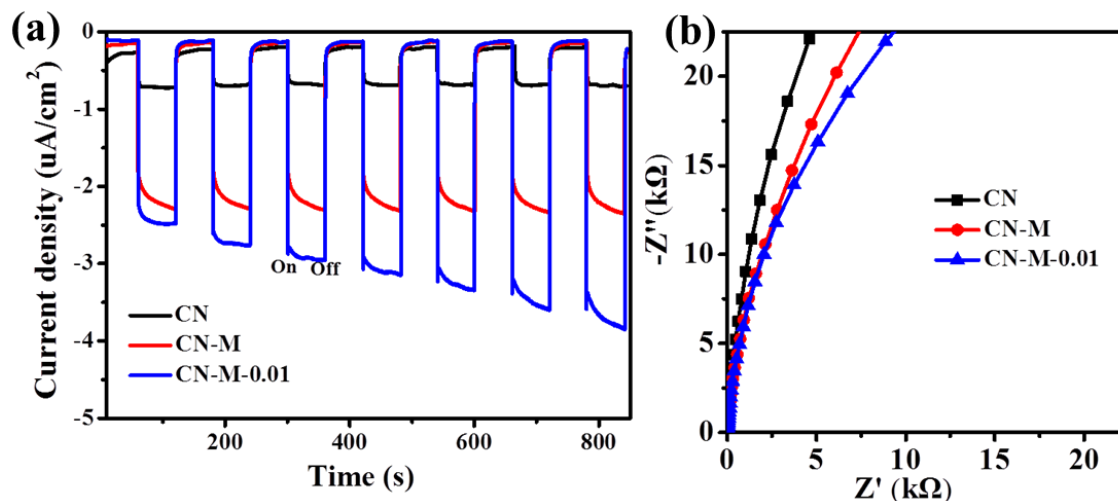
Fig. S10 (a) Transient photocurrent curves and (b) EIS Nyquist plots of CN, CN-M and CN-M-0.01.

The larger photocurrent of CN-M and the largest photocurrent of CN-M-0.01 (Fig. S10a), as well as the smaller semicircular radius of EIS Nyquist plots of CN-M and the smallest semicircular radius of EIS Nyquist plots of CN-M-0.01 (see Fig. S10b) again confirm that both the high crystallinity and defects could improve the charge transfer and separation within carbon nitride, therefore the photoelectrons have more opportunities to participate into the CO_2 reduction reactions. The spike in the photocurrent curve of CN-M-0.01 is caused by the separation of photo-generated electron–hole pairs at the interface of CN-M-0.01/electrode: electrons are transported into the surface because of the surface trap states.
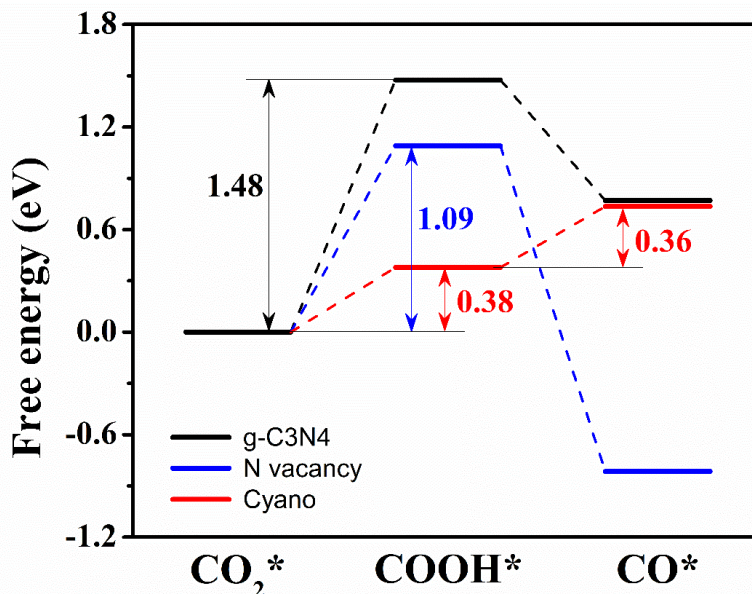
Fig. S11 Gibbs free energy for the conversion of CO_2 into CO on pristine CN-M, CN-M with N vacancy and CN-M with cyano group.

The DFT calculations were used to further understand the origin of high photocatalytic activity. We explored the process of CO_2 into CO by calculating the Gibbs free energy on the pristine CN-M, CN-M with N vacancy and CN-M with cyano group by DFT calculations. As shown in Fig. S11, the CO_2 conversion to COOH* over CN-M with N vacancy and cyano group is more energetically favorable with reference to CN-M, confirming that the N vacancy and cyano group within CN-M could promote the CO_2 conversion to COOH*. During the process of COOH* convert into CO, the energy is also decreased in CN-M with N vacancy, thus indicating the CO_2 reduction promotion by the N vacancy. These DFT calculation results reveal the origin of high photocatalytic activity within CN-M-0.01.

The defects can trap the oxygen atoms from CO_2 molecules, and then activate CO_2 molecules through the high concentration of delocalized electrons.[17] At the same time, H_2O is dissociated into hydroxy groups and protons at the surface. Subsequently, the surface protons can react with the activated CO_2 (CO_2*) to generate COOH*. After that, the photogenerated electrons and protons can interact with COOH* for a further protonation process to produce CO*,[18] while CH_4 and CH_3OH are yielded through a more complex proton-coupled electron-transfer process.[19]
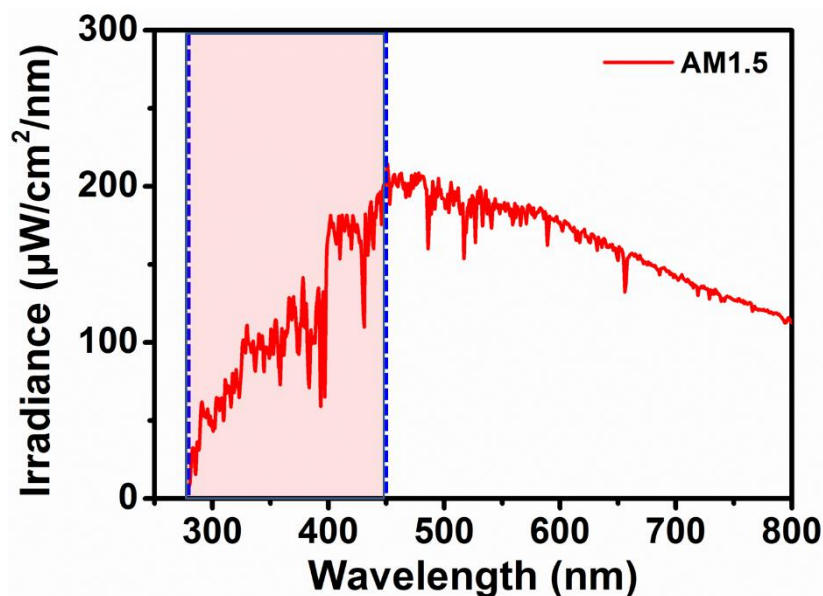
Fig. S12 Light spectrum of the 300 W Xe lamp with an AM1.5 filter. The spectrum was measured at room temperature and at the distance of 5 cm away from the light source, which was the exact distance that the catalyst was immobilized.

References

1   Y. Li, W. Wang, Z. Zhang, M. Woo, C. Wu, P. Biswas, *Appl. Catal. B-Envrion.,* 2010, **100**, 386–392.

2   J. Low, L. Zhang, T. Tong, B. Shen, J. Yu, *J. Catal.*, 2018, **361**, 255–266.

3   P. Xia, M. Antonietti, B. Zhu, T. Heil, J. Yu and S. Cao, *Adv. Funct. Mater.*, 2019, **29**, 1900093.

4   M. Liu, S. Wageh, A. A. Al-Ghamdi, P. Xia, B. Cheng, L. Zhang and J. Yu, *Chem. Commun.*, 2019, **55**, 14023-14026.

5   F. Li, D. Zhang and Q. Xiang, *Chem. Commun.*, 2020, **56**, 2443-2446.

6   B. Liu, L. Ye, R. Wang, J. Yang, Y. Zhang, R. Guan, L. Tian and X. Chen, *ACS Appl. Mater. Interfaces*, 2018, **10**, 4001-4009.

7   J. Fu, K. Liu, K. Jiang, H. Li, P. An, W. Li, N. Zhang, H. Li, X. Xu, H. Zhou, D. Tang, X. Wang, X. Qiu and M. Liu, *Adv. Sci.*, 2019, **6**, 1900796.

8   G. Zhang, G. Li, T. Heil, S. Zafeiratos, F. Lai, A. Savateev, M. Antonietti and X. Wang, *Angew. Chem. Int. Ed.*, 2019, **58**, 3433-3437.

9   Y. Yang, Z. Tang, B. Zhou, J. Shen, H. He, A. Ali, Q. Zhong, Y. Xiong, C. Gao, A. Alsaedi, T. Hayat, X. Wang, Y. Zhou and Z. Zou, *Appl. Catal. B-Envrion.*, 2020, **264**, 118470.

10   S. Tonda, S. Kumar, M. Bhardwaj, P. Yadav and S. Ogale, *ACS Appl. Mater. Interfaces*, 2018, **10**, 2667-2678.

11   X. Wang, K. Maeda, A. Thomas, K. Takanabe, G. Xin, J. M. Carlsson, K. Domen and M. Antonietti, *Nat. Mater.*, 2009, **8**, 76-80.

12   (a) C. Lv, Y. Qian, C. Yan, Y. Ding, Y. Liu, G. Chen and G. Yu, *Angew. Chem., Int. Ed.*, 2018, **57**, 10246-10250; (b) S. Cao, H. Li, T. Tong, H.-C. Chen, A. Yu, J. Yu and H. M. Chen, *Adv. Funct. Mater.*, 2018, **28**, 1802169.

13   W. Ren, J. Cheng, H. Ou, C. Huang, M.-M. Titirici and X. Wang, *ChemSusChem*, 2019, **12**, 3257-3262.

14   W.-J. Ong, L.-L. Tan, Y. H. Ng, S.-T. Yong and S.-P. Chai, *Chem. Rev.*, 2016, **116**, 7159-7329.

15   (a) Z. Chen, A. Savateev, S. Pronkin, V. Papaefthimiou, C. Wolff, M. G. Willinger, E. Willinger, D. Neher, M. Antonietti and D. Dontsova, *Adv. Mater.*, 2017, **29**, 1700555; (b) L. Lin, H. Ou, Y. Zhang and X. Wang, *ACS Catal.*, 2016, **6**, 3921-3931.

16   M. Thommes, K. Kaneko, A. V. Neimark, J. P. Olivier, F. Rodriguez-Reinoso, J. Rouquerol and K. S. Sing, *Pure Appl. Chem.*, 2015, **87**, 1051-1069.

17   (a) W. Wang, H. Zhang, S. Zhang, Y. Liu, G. Wang, C. Sun and H. Zhao, *Angew. Chem. Int. Ed.*, 2019, **58**, 16644-16650; (b) J. Zhang, G. Zhang, X. Chen, S. Lin, L. Moehlmann, G. Dolega, G. Lipner, M. Antonietti, S. Blechert and X. Wang, *Angew. Chem. Int. Ed.*, 2012, **51**, 3183-3187.

18   J. Wu, X. Li, W. Shi, P. Ling, Y. Sun, X. Jiao, S. Gao, L. Liang, J. Xu, W. Yan, C. Wang and Y. Xie, *Angew. Chem. Int. Ed.*, 2018, **57**, 8719-8723.

19   (a) X. Chang, T. Wang and J. Gong, *Energy Environ. Sci.*, 2016, **9**, 2177-2196; (b) Y. Wang, P. Han, X. Lv, L. Zhang and G. Zheng, *Joule*, 2018, **2**, 2551-2582.